ELSEVIER

Journal of Hazardous Materials A75 (2000) 29–46

Journal of Hazardous Materials

www.elsevier.nl/locate/jhazmat

Simple box model for dense-gas dispersion in a straight sloping channel

J.P. Kunsch [a,*], D.M. Webber [b]

[a] *Department of Mechanical Engineering, Swiss Federal Institute of Technology, ETH-Zürich, CH-8092, Zürich, Switzerland*

[b] *Integral Science and Software Ltd., 484 Warrington Rd. Culcheth, Warrington WA3 5RA, UK*

Received 10 November 1999; received in revised form 10 March 2000; accepted 11 March 2000

Abstract

A box model for instantaneous release and subsequent one-dimensional spreading of isothermal dense gases on sloping surfaces is presented. A numerical solution and an approximate analytical solution of the model equations are compared to the experimental data obtained in a sloping heavy-gas channel of the Institute of Fluid Dynamics at ETH-Zürich. The influence of the rear wall of the containment from where the cloud is released is analysed. Different entrainment assumptions, in particular the scaling of the entrainment parameters, are discussed. The numerical values of the entrainment parameters are tuned by computer optimization in order to obtain best agreement of the theoretical results with experimental data.

Keywords: Dense gas; Dispersion; Sloping surface; Box model

1. Introduction

Dense-gas dispersion modelling is an important aspect of risk assessment of chemical installations, used for the production, storage or transportation of hazardous liquids and gases. Nowadays dense-gas dispersion over flat terrain can be predicted reasonably well. However, flat terrain models cannot be used in real situations with buildings and slopes. According to recent reviews (e.g. Britter [1]) the research on simple topographic effects (e.g. straight sloping surfaces) is still of major interest, since a basic understanding of

* Corresponding author.

0304-3894/00/$ - see front matter
PII: S0304-3894(00)00209-0

the fundamental physical phenomena, such as entrainment mechanisms or frontal dynamics on slopes, is still lacking. The few operable computer codes based on numerical models capable of dealing with complex topography or complex terrain are still in the validation process (Hankin [2,3]).

While propagating on slopes, heavy-gas clouds do not only drift downhill but they also change shape. In early models of instantaneously released dense gas clouds proposed, e.g. by Kukkonen and Nikmo [4] the flat terrain integral approach is generalized to include the effect of slope. In these models the slumping is assumed to be unaffected by the convection due to slope (and wind) and the motion of the centroid of the cloud is given by a force balance formulated for the whole cloud. The model presented by Müller and Fanneløp [5] also belongs to this category. Most of these models require numerical computation to obtain a solution and this limits the extent to which one can gain physical insight or a direct interpretation of the parameters involved.

The integral model of Webber et al. [6], where the results of a numerical shallow-layer model are taken into account, for its part yields an analytic solution. Webber et al. restricted themselves to the case of zero wind speed and they neglected mixing with ambient air. They obtained an equation in the one-dimensional and the three-dimensional case for the cloud's terminal velocity down the slope where gravity balances the resistance forces. Müller and Fanneløp [5] compared this equation for the one-dimensional case to the data by Flacher and Müller [7], obtained in a straight sloping channel. The good agreement demonstrates the correct qualitative dependence of the similarity solution of Webber et al. [6] w.r.t. slope angle, released volume and buoyancy. Another important result, already found by means of the shallow-layer model of Webber et al. [6], is the late-time behaviour of the cloud, which gradually adopts the shape of a wedge with horizontal upper surface. Tickle [8] set up a more sophisticated model where the cloud dilution by air entrainment is incorporated. The corresponding entrainment velocity is proportional to the downslope advection velocity. Tickle [8] determined the values of the entrainment coefficient and of the frontal Froude number by fitting the theoretical results relative to concentration and front arrival time to the data of Flacher and Müller [7] and Schatzmann et al. [9]. In Tickle's model the ''top'' and ''wedge'' entrainment terms are proportional for the assumed fixed wedge geometry, so that both entrainment coefficients can be absorbed into a single entrainment coefficient. With his model, Tickle obtains good agreement with experimental data when he assumes a constant coefficient for the entrainment through the top surface. In the present model, however, it appears that the agreement with experimental data can be improved when the entrainment coefficient depends on the slope.

Further experimental data is required not only for validating the models describing the heavy gas dispersion, but also for improving the basic understanding of the physical phenomena. Still very little data exist in case of heavy gas dispersion on slopes. This data would fill gaps of knowledge on which the majority of the international research community agrees. Fanneløp et al., who have been active in the field of safety and environmental flows at ETH-Zürich since 1983, have spent considerable efforts in the investigation of dense-gas dispersion on slopes (Kunsch et al. [10]; Müller and Fanneløp [5]). Attention was focused on heavy-gas dispersion in a calm environment since the related research is well suited for laboratory experiments. The corresponding results are

relevant in risk assessment of installations where heavy gases are involved, because under ‘‘no wind’’ conditions a cloud is slowly diluted and the dangerous concentrations are longer preserved. Experimental data for dense-gas propagation on slopes have been generated at ETH-Zürich in two different types of test facilities: Flacher and Müller [7] released different isothermal heavy gases (Ar, SF_6, CO_2, etc.) on large sloping surfaces, so that the released gas could also extend laterally across the slope. As mentioned earlier, Flacher’s data has been used by Tickle [8], for the numerical tuning of the entrainment coefficient and the leading edge correlation coefficient. Flacher’s experimental observations moreover gave support to the basic assumption of the model that the cloud moving downslope adopts the shape of a wedge, i.e. that the upper surface is almost horizontal. This is also in agreement with the similarity solution, valid for late times, of Webber et al. [6] or Tickle [8].

Two other test facilities, operated by Machacek and Müller [11], consist of straight sloping channels, where the side walls prevent the lateral dispersion. The first channel of 4 m length, 0.6 m width and 0.76 m height can be tilted from 0° to 15°. Prior to release, the heavy gas (Argon) is contained in an initial volume of 0.6 m width and having a shape corresponding to the sketch of Fig. 1. The rear wall consists of a plate of styrofoam™, which can be moved for each experiment to vary the aspect ratio of the cloud at release. The frontal wall consists of a gate, which can be opened manually. The flow can be visualized by adding smoke to the heavy gas. Longer spreading distances are possible in the second channel of 0.5 m width and 8 m length. This channel can be operated with slopes of 0%, 10%, 20% and 30%. Accurate data for the frontal position versus time, obtained by means of aspirated hot-wire probes, and data relative to the time history of the frontal height obtained by visual estimates, is available for different slope angles. This data is used to interpret and validate the model outlined here.

Heavy waste material discharged into coastal sea or snow avalanches (Beghin et al. [12]) are examples of gravity driven flows on sloping ground related to dense-gas dispersion. The classical dam-break problem (Stoker [13]) may be quoted as a related phenomenon in hydraulics. A review of recent research on the dispersion of hazardous materials, including the release and propagation of dense gas clouds on sloping surfaces can be found in Britter [1], where he addressed not only the current state of knowledge but also the major outstanding issues in the field.

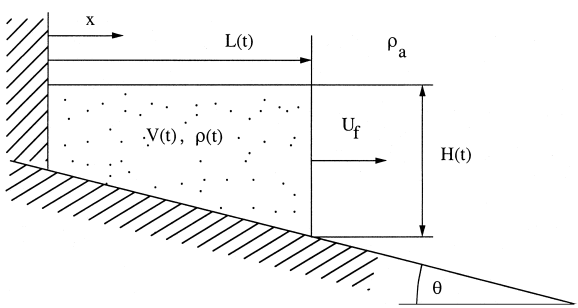

Fig. 1. Side view of the cloud in contact with the rear wall.

2. Box-model of a dense-gas cloud on a sloping surface

The configuration to be modelled in the present contribution is shown in Fig. 1. A volume V_0 of dense gas with initial density ρ_0 at ambient temperature is released instantaneously through a lock-gate located at the coordinate $x = L_0$ into a quiescent ambient with density ρ_a (The quantities at time $t = 0$ have the index 0). At $x = 0$ the cloud is contained by a wall (left-hand side). It is assumed that the top interface is flat. This will be discussed in Section 4.

2.1. Cloud in contact with wall (variant A)

2.1.1. Equations and basic assumptions

The basic equations are formulated for the planar case (with unit width $W = 1$), corresponding to a sloping channel flow. The detailed developments can be found in Kunsch et al. [14].

Since isothermal gases are considered, the buoyancy is conserved

$$B = g' V = g'_0 V_0 = \text{const.} \tag{1}$$

V represents the volume of gas, $g' = g(\rho - \rho_a)/\rho_a$ corresponds to the reduced gravitational acceleration and the index $(\,)_0$ denotes the conditions at release at time $t = 0$.

The reference quantities

$$L_{ref} = \sqrt{V_0}\,, \quad U_{ref} = \sqrt{g'_0 L_{ref}} = (Bg'_0)^{1/4} \quad \text{and} \quad t_{ref} = L_{ref}/U_{ref} \tag{2}$$

can be defined in order to formulate the model equations in non-dimensional form. The non-dimensional geometric quantities are $\nu = V/L_{ref}^2$; $h = H/L_{ref}$; $l = L/L_{ref}$ and the non-dimensional time is $\tau = t/t_{ref}$. We will further use the abbreviation $\Gamma = \tan(\theta)$.

The frontal speed corresponds to the familiar gravity–current relation (Fanneløp [15]), which reads in dimensional form $U_f = k\sqrt{g'H}$. k is an empirical frontal factor to be discussed in Section 4. The non-dimensional form of the frontal speed reads

$$u_f = k\sqrt{\frac{h}{\nu}} = \frac{\mathrm{d}l}{\mathrm{d}\tau} \tag{3}$$

The volume of gas mixture is

$$\nu = lh - \frac{1}{2}\Gamma l^2 \tag{4}$$

The dilution of the initially released gas volume is due to air entrainment, which is scaled with the frontal area of the cloud

$$\frac{\mathrm{d}\nu}{\mathrm{d}\tau} = \kappa h u_f \tag{5}$$

The choice of this entrainment assumption and the correlation of the model results with experimental data will be discussed in Section 4.

The model variant A is valid as long as the height of the rear part of the cloud has a positive value, i.e.

$$h - l\Gamma > 0 \tag{6}$$

2.1.2. Solution of the equations

The solution procedure of the system of Eqs. (3)–(5) is outlined in Appendix A. It results for the frontal height versus frontal position

$$\frac{h}{l_0} = \left(\frac{h_0}{l_0} - \frac{\Gamma}{2-\kappa}\right)\left(\frac{l}{l_0}\right)^{\kappa-1} + \frac{\Gamma}{2-\kappa}\left(\frac{l}{l_0}\right) \tag{7}$$

The volume is also given as a function of the frontal position

$$\frac{\nu}{l_0^2} = \left(\frac{h_0}{l_0} - \frac{\Gamma}{2-\kappa}\right)\left(\frac{l}{l_0}\right)^{\kappa} + \frac{\Gamma\kappa}{2(2-\kappa)}\left(\frac{l}{l_0}\right)^2 \tag{8}$$

The time corresponding to a position of the front $Y = l/l_0$ is given by

$$\tau = c_6\left\{\left(Y^{3/2} - 1\right) + \sum_{n=1}^{\infty} C_n\left[Y^{3/2}\left(\frac{\varepsilon Y^{2-\kappa}}{1+\varepsilon Y^{2-\kappa}}\right)^n - \left(\frac{\varepsilon}{1+\varepsilon}\right)^n\right]\right\} \tag{9}$$

where $\varepsilon = \Gamma/[(h_0/l_0)(2-\kappa) - \Gamma]$; and $c_6 = (2/3)(l_0^{3/2}/k)$.

Here τ is an explicit function of $Y = l/l_0$. The value of l depending on τ can be read from Figs. 3, 4 or 6 below. The accuracy is of the order of 1% to 2% when three terms of the summation are taken into account. The coefficients C_n are given in Appendix A.

2.1.3. Validity range of model variant A

The model is valid as long as the rear part of the cloud is in contact with the wall, i.e. as long as the inequality (6) is fulfilled. When h/l_0 given by Eq. (7) is substituted into the inequality (6) we obtain the range of the front position for which the model variant A is applicable, i.e.:

$$1 \le \frac{l}{l_0} < \left(\frac{l}{l_0}\right)_{\text{crit.}} \qquad \text{where } \left(\frac{l}{l_0}\right)_{\text{crit.}} = Y_{\text{crit.}} = \left[\frac{(1-\kappa)\,\Gamma}{(2-\kappa)\,h_0/l_0 - \Gamma}\right]^{1/(\kappa-2)} \tag{10}$$

The corresponding critical time $\tau_{\text{crit.}}$ can be obtained when $Y_{\text{crit.}}$ is substituted into Eq. (9).

2.2. Cloud not in contact with the rear wall (variant B)

2.2.1. Equations and basic assumptions

The situation when the rear part of the cloud has lost contact with the wall is depicted in Fig. 2. Now the rear edge (or ''tail'') of the cloud travels with velocity $U_t = \mathrm{d}L_t/\mathrm{d}t$

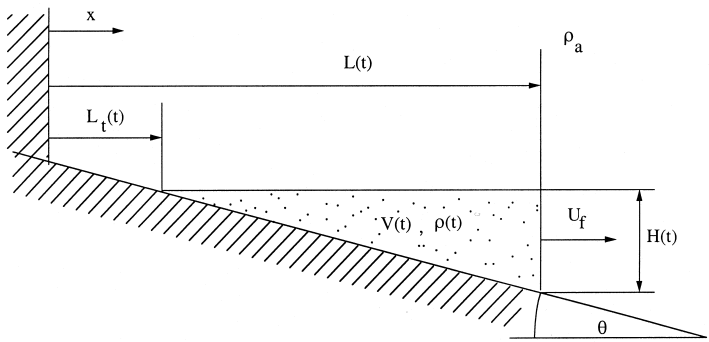

Fig. 2. Side view of the cloud not in contact with the rear wall.

and the top surface is again assumed to be horizontal. The geometry of the cloud of variant B is described now by the following non-dimensional equations:

$$\text{frontal height: } h = \Gamma(l - l_t) \tag{11}$$

$$\text{volume of gas mixture: } \nu = \frac{1}{2}\Gamma(l - l_t)^2 \tag{12}$$

The model equations for the frontal dynamics and for the cloud dilution by front entrainment correspond to Eqs. (3) and (5) of model variant A.

2.2.2. Solution of the equations

Considering that $u_f = \mathrm{d}l/\mathrm{d}\tau$ and $u_t = \mathrm{d}l_t/\mathrm{d}\tau$, Eqs. (11) and (12) both, are substituted into the differential Eq. (5) to obtain

$$u_t = Gu_f \qquad \text{where } G = 1 - \kappa \tag{13}$$

and it follows that

$$l_t = G(l - l_{\text{crit.}}) \tag{14}$$

as $l_t = 0$ when $l = l_{\text{crit.}}$.

With the help of Eq. (14) l_t can be eliminated from both Eqs. (11) and (12), which are substituted into the frontal condition $u_f = \mathrm{d}l/\mathrm{d}\tau = k\sqrt{h/\nu}$ in order to obtain a differential equation w.r.t. l.

The solution, which includes the initial condition given by Eq. (10), is straightforward:

$$\tau = \tau_{\text{crit.}} + \frac{1}{k\kappa}\frac{\sqrt{2}}{3}\left\{\left[\kappa l + (1-\kappa)l_{\text{crit.}}\right]^{3/2} - l_{\text{crit.}}^{3/2}\right\} \tag{15}$$

or

$$l = \frac{1}{\kappa}\left\{\left[\frac{3}{\sqrt{2}}k\kappa(\tau - \tau_{\text{crit.}}) + l_{\text{crit.}}^{3/2}\right]^{2/3} - (1-\kappa)l_{\text{crit.}}\right\} \tag{16}$$

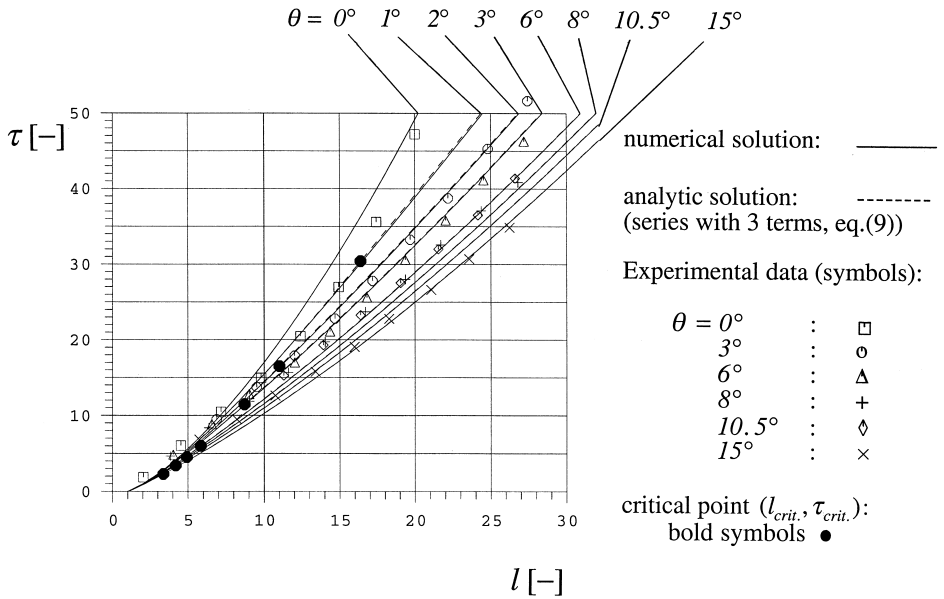

Fig. 3. Range of the cloud versus time for different slope angles θ (results given in non-dimensional form) (entrainment parameter: $\kappa = 0.25$).

The height of the front can be deduced when Eqs. (14) and (16) are substituted into Eq. (11). $l_{\text{crit.}}$ is given by Eq. (10) in Section 2.1. $\tau_{\text{crit.}} = \tau(l_{\text{crit.}})$ follows from Eq. (9). The

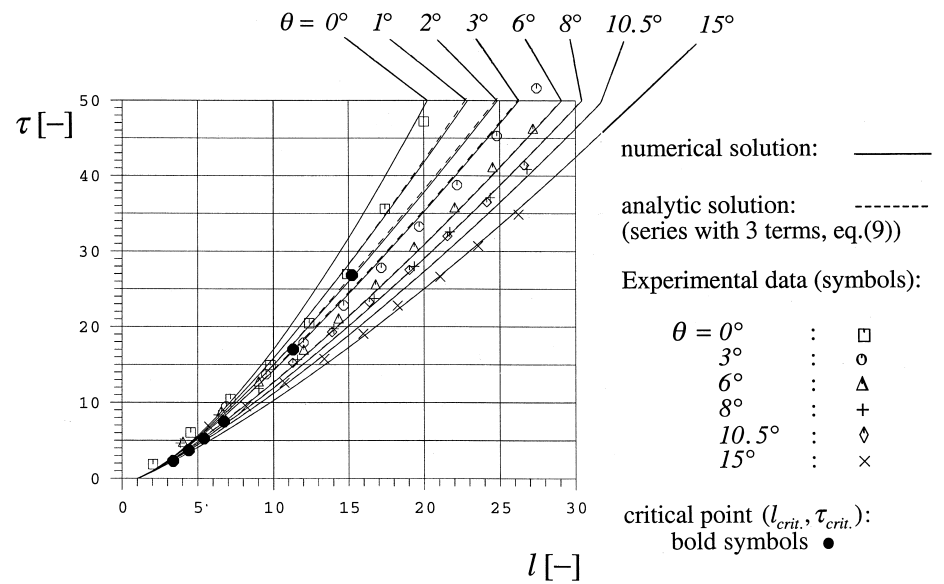

Fig. 4. Range of the cloud versus time for different slope angles θ (results given in non-dimensional form) (entrainment parameter depending on slope: $\kappa = \kappa_0/(1+\delta\Gamma)$; $\kappa_0 = 0.45$, $\delta = 3$).

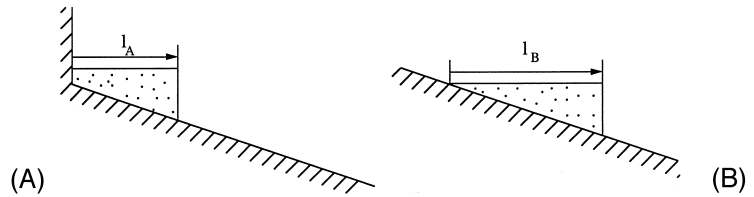

Fig. 5. Real (A) and idealized (B) configuration for the approximate solution.

range of the cloud versus time for different slope angles is shown in non-dimensional form in Fig. 3 for the constant entrainment parameter $\kappa = 0.25$ and in Fig. 4 for the entrainment parameter κ which depends on the slope angle: $\kappa = \kappa_0/(1 + \delta\Gamma)$ with $\kappa_0 = 0.45$ and $\delta = 3$. The choice of the parameters will be discussed in Section 4. The critical point (l_{crit}, $\tau_{\text{crit.}}$) is indicated by the bold symbols in Fig. 3 and in Fig. 4. The deviation of the approximate solution by series from the exact solution of variant A increases with time until $\tau = \tau_{\text{crit.}}$. For this reason the deviation is most relevant for small slope angles with large $\tau_{\text{crit.}}$. For times $\tau > \tau_{\text{crit.}}$ the analytic solution is exact, where the initial condition $\tau_{\text{crit.}}$ is given by the approximate solution of variant A, i.e. Eq. (9) $\tau_{\text{crit.}} = \tau(l_{\text{crit.}})$.

3. Approximate solution

In the case where no rear wall is present at release, the solution for model variant B, given by Eq. (15) or (16), is valid almost from the beginning, i.e. for times shortly after the initial slumping motion. If a rear wall is present at release, the model variant A is applicable until the moment $\tau_{\text{crit.}}$ when the tail of the cloud loses contact with the rear wall. We have found an approximate solution for large slope angles (exceeding about 5°) so that the rather laborious evaluation of the summation in Eq. (9) can be avoided. The real cloud sketched in Fig. 5A to be treated here is idealized by a wedge-shaped cloud in Fig. 5B which can actually be observed at later times. Taking equal initial volume and equal initial buoyancy in both cases, the starting frontal position for the real case can be related to that for the idealized case by the following formula

$$l_{\text{B}}(\tau = 0) = l_{\text{A}}(\tau = 0)\sqrt{\frac{2\text{AR} - \Gamma}{\Gamma}} \tag{17}$$

with the aspect ratio at release $\text{AR} = (h/l)_{\tau=0} = h_0/l_0$.

The crude assumption made in the present approximate solution is that the initial lead $l_{\text{B}}(\tau = 0) - l_{\text{A}}(\tau = 0)$ of the front of model variant B over the front of variant A is valid for all times $\tau > 0$: $l_{\text{B}}(\tau) - l_{\text{A}}(\tau) = l_{\text{B}}(\tau = 0) - l_{\text{A}}(\tau = 0)$, i.e.

$$l_{\text{B}} = l_{\text{A}} + \left[l_{\text{B}}(\tau = 0) - l_{\text{A}}(\tau = 0)\right] \tag{18}$$

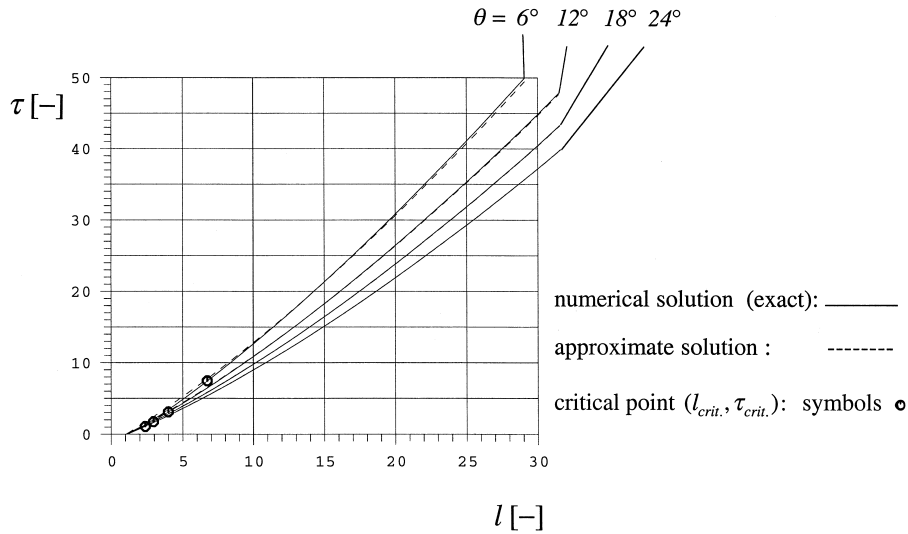

Fig. 6. Range of the cloud versus time for different slope angles θ (numerical solution and approximate solution).

This expression can be substituted into Eq. (16) to obtain the frontal position l_A of the real cloud corresponding to Fig. 5A and later to Fig. 5B:

$$l_A = l_A(\tau = 0) + \frac{1}{\kappa}\left\{\left[\frac{3}{\sqrt{2}} k\kappa\tau + l_B^{3/2}(\tau = 0)\right]^{2/3} - l_B(\tau = 0)\right\} \tag{19}$$

or explicitly w.r.t. τ:

$$\tau = \frac{\sqrt{2}}{3}\frac{1}{k\kappa}\left\{\left[\kappa\left(l_A - l_A(\tau = 0)\right) + l_B(\tau = 0)\right]^{3/2} - l_B^{3/2}(\tau = 0)\right\} \tag{20}$$

where $l_B(\tau = 0)$ is given by Eq. (17).

The approximate solution is compared to the exact solution in Fig. 6. The accuracy of the approximation increases with increasing slope angle. The reason is that for large slope angles the cloud is in contact with the rear wall for a short time interval after release only. In this case the model variant A, which is neglected in the approximate solution, is relevant only for the corresponding short duration $\tau_{crit.}$ indicated by the bold symbols in Fig. 6.

4. Discussion

An enclosure around a potential dense-gas spill can shield the surrounding regions, such as dwellings close to a process plant, from possible hazardous emissions. Obstacles like barriers or fences would prevent dense-gas clouds from spreading in a (possibly sloping) street canyon. The situation in the laboratory can be imagined as a rather crude

idealization of a real scenario, where a fence is partially and suddenly removed by accident or inadvertence. In addition, it is assumed that the initial momentum, due to a possibly high pressure release from the containment, has been dissipated in the enclosure prior to the removal of the fence. Due to the presence of the fixed side walls and the fixed rear wall, the evacuation process of the starting element is partly prevented, so that the total height of the cloud decreases more slowly than in the case when all the walls are removed simultaneously. A larger height of the cloud, as compared to a release without side walls, results in a higher frontal speed of the cloud. In particular for large slope angles we have shown that the cloud is in contact with the rear wall for very short time only, so that the exact release configuration must not be known for practical applications. On the other hand, well defined geometrical characteristics and time parameters have to be taken into account when a consistent comparison of the theoretical results to the experimental data is required.

In the present model it is implicitly assumed that the top interface is flat. This is not in agreement with the results of Webber et al. [6], who gave a numerical description of the release of a wedge shaped cloud and the subsequent spreading without mixing. The initial expansion wave, generated at the moment of release and reflected at the rear wall, ends with a system of waves and the formation of a hydraulic jump, separating a ''tail'' and a ''head'' region. This jump collapses after the front has travelled a distance equal to 10 times the initial cloud length, so that a smooth top surface is obtained. However, when mixing is incorporated in the model, the inertia of the entrained air damps the internal waves (see e.g. Kunsch [16]). In this case a smooth top surface can be observed almost from the beginning on, which makes the assumption of a flat top surface realistic.

The frontal Froude number can be more or less strongly influenced by different factors, e.g. the air entrainment, the Reynolds number or the slope angle.

Air entrainment: In the simple gravity–current formula for the frontal speed it is assumed that the flow is driven by the hydrostatic pressure difference across the frontal region. It can be shown by simple physical arguments (see Fanneløp [15] for a review) that the frontal speed of isothermal dense gases spreading over a horizontal surface, is independent of the dilution or air entrainment into the cloud.

Reynolds number: Even for equal slopes, the frontal Froude numbers can differ considerably when different gases are considered. Here it is referred to Flacher's data documenting downslope motion of dense gases (Argon and Freon) combined with lateral spreading across the slope. According to Flacher and Müller [7] and Tickle [8], an influence of the Reynolds number on the flow may be responsible for this discrepancy. Since only data for releases of Argon in sloping channels is available, a generalization of the range of validity of the frontal Froude number to other gases is excluded at present.

Slope angle: In addition, given the limited experimental data available, a possible slope–angle dependence of the frontal Froude number cannot clearly be identified. Tickle came to the same conclusion in the context of his model, dealing with downslope motion of dense gases including lateral spreading across the slope. Best agreement of the theoretical frontal position with experimental data has been obtained by numerical tuning of the frontal factor k. The value of the frontal factor equal to 1.2, which is independent of the entrainment characteristics, is close to the value obtained by Billeter and Fanneløp [18] for one-dimensional spreading in a horizontal channel.

Initial acceleration: The experimental data relating to the frontal position versus time reveal that the initial motion produced by the box model is too slow. By assuming that the front velocity is a function of the potential energy available, an improved model (Müller and Fanneløp [5]) could be obtained, where the effect of the vertical velocities during the slumping motion is taken into account. As an alternative, Van Ulden's model [17] could be applied, where the initial acceleration is accounted for. The corresponding analysis including a comparison with experimental data can be found in Billeter and Fanneløp [18] in the context of horizontal channel flow. The present model could be improved for early times by incorporating a (possibly slope dependent) time shift. Since

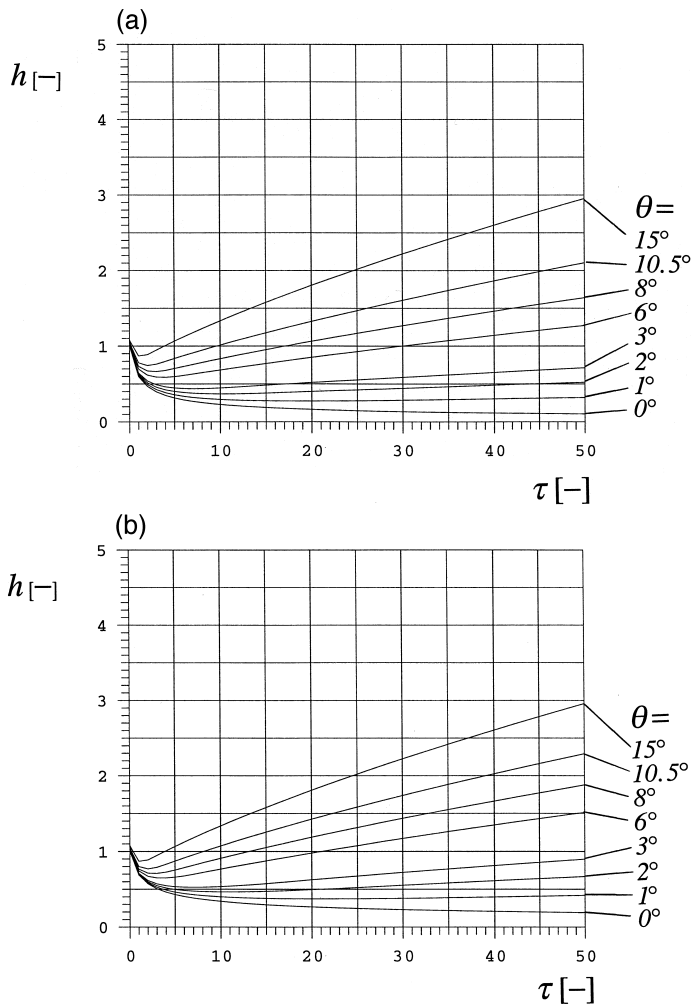

Fig.7. Height of the front versus time for different slope angles θ. (a) theory with $\kappa = 0.25$; (b) theory with $\kappa = \kappa_0/(1+\delta\Gamma)$; $\kappa_0 = 0.45$, $\delta = 3$.

such an additional parameter would be introduced at the expense of the simplicity of the model, it will not be taken into consideration.

Two correlations based on different values for the entrainment parameters will be considered. The corresponding frontal ranges are shown in Fig. 3 and in Fig. 4, respectively. In both cases the values have been chosen to obtain a best fit of the model results to the experimental data for the largest slope angle considered in the experiments, i.e. $\theta = 15°$. In the first case, the value of the entrainment parameter is constant: $\kappa = 0.25$. It can be shown by comparison of the theoretical results to the experimental data (Fig. 3) that for small slope angles the theoretical frontal velocity is too sensitive to small variations of the slope angle. The overprediction of the frontal range for small slope angles, as observed in Fig. 3, can be reduced by increasing the resistance force or the front entrainment parameter for small θ, i.e. $\kappa = \kappa_0/(1 + \delta\Gamma)$ (see Fig. 4). It is felt that parameters in addition to κ_0 and δ, which would be introduced at the expense of the simplicity of the model, would hardly bring an improvement to the accuracy of the correlation.

The comparison of the theoretical frontal height with experimental data could yield an additional argument in favour of the variant where the entrainment parameter depends on the slope angle (Fig. 4). In particular, for small slope angles the rapid increase of the frontal height observed in the experiments is better taken into account when a slope angle dependence is considered. So, the theory with an entrainment parameter depending on the slope yields a frontal height which is about 20% larger than the height predicted by a theory with constant κ, when angles smaller than 3° and the (dimensionless) time $\tau = 50$ are considered (Fig. 7). Only qualitative agreement of the theoretical results with experimental data can be required for the frontal height, since the

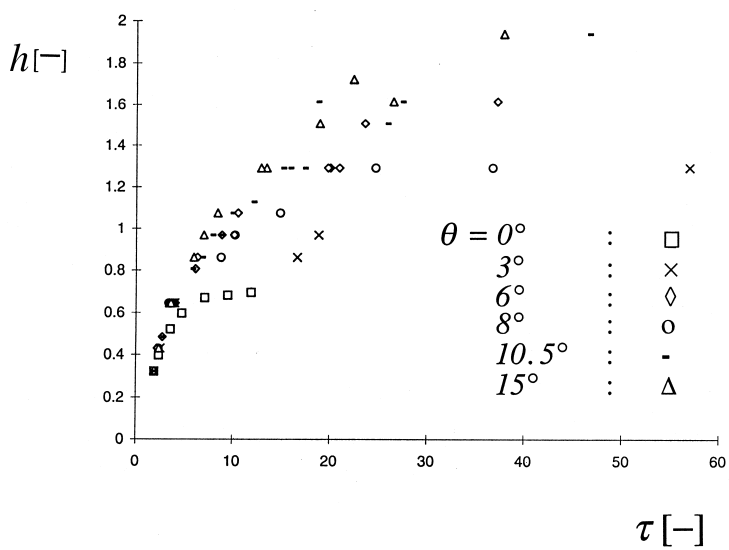

Fig. 8. Height of the front versus time for different slope angles θ, experiment by Machacek and Müller [11] (visual observations).

latter has been determined by visual observations subject to a greater inaccuracy than the measurements of the frontal range. In addition, it is demonstrated in Fig. 8 that the initial slumping motion could not be recorded, mostly due to its short duration.

There is still some discussion about the real physics governing the entrainment process, i.e. whether dilution should be attributed to top entrainment or to front entrainment. In the present box model, it could be shown formally that the contribution to the top entrainment has to be small for small θ and that it must vanish for horizontal spreading. The physical reason is that the top entrainment would violate the principle of energy conservation for horizontal spreading in a calm environment due to the defined amount of potential energy available and the unbounded rise of the centre of gravity of the cloud. On the other hand, the centre of gravity can rise when the wind contributes to the addition of turbulent kinetic energy mostly through the top surface of the cloud. In the light of the latter observations the designations ''gravity powered entrainment'' and ''wind powered entrainment'' would be more appropriate than front entrainment and top entrainment, respectively, in agreement with former discussions of Webber and Wheatley [19]. Since the experimental data used for the set up of the present correlations were obtained in a calm laboratory environment, the entrainment assumption based on the scaling with the frontal area will be the most appropriate.

5. Conclusions

The experimental observation and the theoretical result from previous numerical analyses that the top surface of heavy gas clouds on sloping surfaces remains horizontal represents a useful element of the present box model.

The simple model presented here does not allow detailed modelling of all the physical phenomena contributing to the dilution of the cloud. However, it does recognise that there are two phases of slumping and dilution — an initial slumping phase with a changing aspect ratio and a later downhill travel phase — and treats them both. These phases were recognised in the work of Webber et al. [6] but they treated only the second. The existence of the first phase, and the associated dilution, means that both phases should really be considered if one is going to fit data.

The second phase is characterised by a self-similar shape (in our approximation) in which the top and front areas scale in proportion. The distinction between separate ''top'' and ''edge'' entrainment mechanisms encountered in models of dispersion on flat terrain is therefore confined to the first phase. However, in the windless conditions studied here energy conservation considerations limit the process to edge entrainment (gravity powered entrainment scaling with the frontal area) even in the first phase. For this reason, a single entrainment parameter is used here. It is allowed to vary with slope and is used to correlate the model results with experimental data.

The experimental information on cloud concentration is unsatisfactory due to the lack of accuracy in the determination of the frontal height. This represents a major shortcoming of the present model, since the gas concentration, rather than the front arrival time, is of key interest for tuning adequately the entrainment coefficient.

We used a value for the k factor in the gravity-intrusion formula which is close to the value found by Billeter and Fanneløp [18] for horizontal spreading of isothermal gases. The generalization of this value to spreading scenarios with slope angles, for lack of better and above all simple information, is questionable.

The influence of the cloud geometry at release, differing from the shape of a wedge and including a fixed wall opposite to the spreading direction downhill, has been analysed. The influence of the rear wall is less important for large slope angles than for small slope angles because the time interval when the cloud is in contact with the rear wall is shorter.

The analytic solution, obtained at the expense of the detailed modelling of the different physical phenomena, represents a useful tool for the safety engineer, because it allows rapid estimates of the frontal range of isothermal clouds on sloping surfaces. An approximate, but simple solution has proven to be rather accurate for slope angles exceeding 5°.

Nomenclature

AR	aspect ratio at release, $\mathrm{AR} = h_0/l_0$
B	buoyancy of the cloud, $B = g'V$
g	gravitational acceleration
g'	reduced gravitational acceleration, $g' = g(\rho - \rho_a)/\rho_a$
h	dimensionless height of the cloud at the front, $h = H/L_{\mathrm{ref}}$
h_0	h at release
H	height of the cloud at the front
k	empirical frontal factor, front Froude number, cf. Eq. (3)
l	dimensionless distance of the front from the rear wall, $l = L/L_{\mathrm{ref}}$
l_0	l at release
l_t	dimensionless L_t
L	distance of the front of the cloud from the rear wall
L_0	L at release
L_{ref}	reference length, $L_{\mathrm{ref}} = \sqrt{V_0}$
L_t	distance of the rear side (tail) of the cloud from the rear wall
t	time
t_{ref}	reference time, $t_{\mathrm{ref}} = L_{\mathrm{ref}}/U_{\mathrm{ref}}$
u_f	dimensionless frontal velocity
U_f	frontal velocity of the cloud
U_t	velocity of the tail of the cloud
U_{ref}	reference speed, $U_{\mathrm{ref}} = \sqrt{g'_0 L_{\mathrm{ref}}}$
ν	dimensionless volume of the cloud
ν_0	ν at release
V	Volume of the cloud
V_0	Volume of the cloud at release
x	distance from the rear wall
Y	$Y = l/l_0$

Greek letters

Γ	$\Gamma = \tan(\theta)$
ε	parameter related to slope angle, cf. Eq. (9)
θ	slope angle of the surface on which the cloud spreads
κ	parameter for the entrainment scaled with the frontal area
ρ	density of the cloud
ρ_0	density of the cloud at release
ρ_a	ambient density
τ	dimensionless time $\tau = t/t_{ref}$

Appendix A. Solution of the equations of model variant A

τ is eliminated from Eqs. (3) and (5) to obtain:

$$\frac{d\nu}{dl} = \kappa h \tag{A1}$$

Eq. (4) is derived w.r.t. l:

$$\frac{d\nu}{dl} = h + l\frac{dh}{dl} - \Gamma l \tag{A2}$$

$d\nu/dl$ is eliminated from Eqs. (A1) and (A2) in order to obtain a differential equation for h where l is the independent variable. With the initial conditions for the length $l(\tau = 0) = l_0$ and the height $h(\tau = 0) = h_0$, the solution of the differential equation is given by

$$\frac{h}{l_0} = \left(\frac{h_0}{l_0} - \frac{\Gamma}{2-\kappa}\right)\left(\frac{l}{l_0}\right)^{\kappa-1} + \frac{\Gamma}{2-\kappa}\left(\frac{l}{l_0}\right) \tag{A3}$$

Eq. (A3) can be substituted into Eq. (4) to obtain the dimensionless volume

$$\frac{\nu}{l_0^2} = \left(\frac{h}{l_0} - \frac{\Gamma}{2-\kappa}\right)\left(\frac{l}{l_0}\right)^{\kappa} + \frac{\Gamma\kappa}{2(2-\kappa)}\left(\frac{l}{l_0}\right)^2 \tag{A4}$$

When Eqs. (A3) and (A4) are substituted into Eq. (3) we obtain:

$$\left[1 + \left(\frac{\kappa}{2} - 1\right)\frac{\varepsilon Y^{2-\kappa}}{1 + \varepsilon Y^{2-\kappa}}\right]^{1/2} Y^{1/2} dY = \frac{k}{l_0^{3/2}} d\tau = \frac{2}{3}\frac{1}{c_6} d\tau \tag{A5}$$

where $\varepsilon = \Gamma/[(h_0/l_0)(2-\kappa) - \Gamma]$ and $c_6 = (2/3)(l_0^{3/2}/k)$.

The new dependent variable is $Y = l/l_0$.

The solution of the differential Eq. (A5), which can be found in Appendix B, reads

$$f(Y) = Y^{3/2}\left[1 + \sum_{n=1}^{\infty} C_n\left(\frac{\varepsilon Y^{2-\kappa}}{1 + \varepsilon Y^{2-\kappa}}\right)^n\right] = \frac{1}{c_6}\tau + c' \tag{A6}$$

c' can be evaluated with the help of the initial condition $Y(\tau = 0) = 1$. Eq. (A6) then becomes:

$$\tau = c_6 \left\{ (Y^{3/2} - 1) + \sum_{n=1}^{\infty} C_n \left[Y^{3/2} \left(\frac{\varepsilon Y^{2-\kappa}}{1 + \varepsilon Y^{2-\kappa}} \right)^n - \left(\frac{\varepsilon}{1+\varepsilon} \right)^n \right] \right\} \tag{A7a}$$

where

$$C_n = \frac{\alpha}{n} \sum_{k=1}^{n} \omega_k \left(\prod_{i=k}^{n} \frac{i}{i+\alpha} \right)$$

with

$$\omega_k = \binom{1/2}{k} \left(\frac{\kappa}{2} - 1 \right)^k = \frac{\left(\frac{1}{2}\right)\left(-\frac{1}{2}\right)\left(-\frac{3}{2}\right) \cdots \left(\frac{3}{2} - k\right)}{k!} \left(\frac{\kappa}{2} - 1 \right)^k$$

and

$$\alpha = \frac{3}{2(2-\kappa)}$$

The coefficients C_n can be evaluated by a recursive procedure:

$$C_n = \frac{1}{n+\alpha} \left[(n-1) C_{n-1} + \alpha \omega_n \right] \tag{A7b}$$

The accuracy is of the order of 1% to 2% when three terms of the summation are taken into account. The first coefficients are as follows:

$$C_0 = \frac{1}{2}\left(1 - \frac{\kappa}{2}\right); \quad C_1 = \frac{1}{1+\alpha}(-\alpha C_0);$$

$$C_2 = \frac{1}{2+\alpha}\left(C_1 - \frac{1}{2}\alpha C_0^2\right); \quad C_3 = \frac{1}{3+\alpha}\left(2C_2 - \frac{1}{2}\alpha C_0^3\right)$$

Appendix B. Solution of Eq. (A5) relative to model variant A

When $x^{1/\alpha} = \varepsilon Y^{2-\kappa}$ (with $\alpha = 3/2(2-\kappa)$) is substituted into Eq. (A5) we obtain

$$\left[1 + \left(\frac{\kappa}{2} - 1 \right) \frac{x^{1/\alpha}}{1 + x^{1/\alpha}} \right]^{1/2} \mathrm{d}x = \frac{\varepsilon^{\alpha}}{c_6} \mathrm{d}\tau \tag{B1}$$

Since $|z| = |((\kappa/2) - 1) x^{1/\alpha}/(1 + x^{1/\alpha})|$ is always smaller than unity, a Taylor series is developed w.r.t. z, i.e.

$$\left[1 + \sum_{n=1}^{\infty} \omega_n \left(\frac{x^{1/\alpha}}{1 + x^{1/\alpha}} \right)^n \right] \mathrm{d}x = \frac{\varepsilon^{\alpha}}{c_6} \mathrm{d}\tau \qquad \text{where } \omega_n = \binom{1/2}{n} \left(\frac{\kappa}{2} - 1 \right)^n \tag{B2}$$

or

$$x + \sum_{n=1}^{\infty} \omega_n \int \left(\frac{x^{1/\alpha}}{1 + x^{1/\alpha}} \right)^n \mathrm{d}x = \frac{\varepsilon^{\alpha}}{c_6} \tau + c' \tag{B3}$$

When the integral in Eq. (B3) is evaluated by parts we obtain

$$\int \left(\frac{x^{1/\alpha}}{1 + x^{1/\alpha}} \right)^n \mathrm{d}x = \alpha x \sum_{k=0}^{\infty} \frac{1}{n+k} \left(\frac{x^{1/\alpha}}{1 + x^{1/\alpha}} \right)^{n+k} \left(\prod_{i=0}^{k} \frac{n+i}{n+\alpha+i} \right) \tag{B4}$$

Further algebraic rearrangements of Eqs. (B3) and (B4) lead to

$$x \left[1 + \sum_{n=1}^{\infty} C_n \left(\frac{x^{1/\alpha}}{1 + x^{1/\alpha}} \right)^n \right] = \frac{\varepsilon^{\alpha}}{c_6} \tau + c'$$

or

$$Y^{3/2} \left[1 + \sum_{n=1}^{\infty} C_n \left(\frac{\varepsilon Y^{2-\kappa}}{1 + \varepsilon Y^{2-\kappa}} \right)^n \right] = \frac{1}{c_6} \tau + c''$$

where

$$C_n = \frac{\alpha}{n} \sum_{k=1}^{n} \omega_k \left(\prod_{i=k}^{n} \frac{i}{i+\alpha} \right)$$

References

[1] R.E. Britter, Recent research on the dispersion of hazardous materials, Industrial safety, environment and climate programme, Final Report of European Commission Contract No. ENV4-CT95-4001 (1998), publication of the European Commission EUR 18198 EN.

[2] R.K.S. Hankin, Comparison of the TWODEE model against the Mercer et al. heavy gas dispersion code comparison exercise. Technical report RAS/96/19, 1996, Health and Safety Laboratory, Broad Lane, Sheffield S3 7HQ.

[3] R.K.S. Hankin, Heavy gas dispersion over complex terrain, PhD thesis, Cambridge University, 1997.

[4] J. Kukkonen, J. Nikmo, Modelling heavy gas cloud transport in sloping terrain, Journal of Hazardous Materials 31 (1992) 155–176.

[5] J. Müller, T.K. Fanneløp, Experimental study of heavy-gas dispersion on sloping surfaces, in: Mixing and Dispersion of Stably Stratified Flows, Fifth IMA Conference on Stratified Flows, Dundee, Sept., 1996.

[6] D.M. Webber, S.J. Jones, D. Martin, A model of the motion of a heavy gas cloud released on a uniform slope, Journal of Hazardous Materials 33 (1993) 101–122.

[7] A. Flacher, J. Müller, Experimentelle Untersuchung der Ausbreitung einer Schwergaswolke auf geneigtem Grund, Diploma Thesis supervised by J.Müller and T.K. Fanneløp, Institut für Fluiddynamik, ETH Zürich, 1994.

[8] G.A. Tickle, A model of the motion and dilution of a heavy gas cloud released on a uniform slope in calm conditions, Journal of Hazardous Materials 49 (1996) 29–47.

[9] M. Schatzmann, K. Marotzke, J. Donat, Research on continuous and instantaneous heavy gas clouds — contribution of sub-project EV4T-00210D to the final report of the joint CEC project, University of Hamburg, Meteorological Institute Report, 1990.

[10] J.P. Kunsch, H.P. Gröbelbauer, L. Billeter, T.K. Fanneløp, Schwergasforschung an der ETH-Zürich, in: S. Hartwig (Ed.), IV Symposion ''Schwere Gase und Sicherheitsanalyse'', Bonn 26./27.09, 1991.
[11] M. Machacek, J. Müller, Untersuchungen zur instationären Ausbreitung von Schwergaswolken in einem geneigten Kanal, Semester Project supervised by J.Müller and T.K.Fanneløp, Institut für Fluiddynamik, 1996.
[12] P. Beghin, E.J. Hopfinger, R.E. Britter, Gravitational convection from instantaneous sources on inclined boundaries, Journal of Fluid Mechanics 31 (1981) 209–248.
[13] J.J. Stoker, Water Waves, Interscience, 1957.
[14] J.P. Kunsch, D.M. Webber, Simple box model for dense-gas dispersion in a straight sloping channel, Internal report IFD-IB 99-3, Institute of Fluiddynamics Swiss Federal Institute of Technology, 1998.
[15] T.K. Fanneløp, Fluid mechanics for industrial safety and environmental protection, in: Industrial Safety Series Vol. 3 Elsevier, Amsterdam, 1994.
[16] J.P. Kunsch, Integralverfahren der Fluiddynamik zur Berechnung von Gasausbreitung und Quellprozessen als Werkzeuge des Sicherheitsingenieurs, Habilitation thesis, Swiss Federal Institute of Technology, 1997.
[17] A.P. Van Ulden, The spreading and mixing of a dense cloud in still air, in: Proc. Stably Stratified Flow and Dense Gas Dispersion, Chester, 1988.
[18] L. Billeter, T.K. Fanneløp, Concentration measurements in dense isothermal gas clouds with different starting conditions, Atmospheric Environment 31 (5) (1997) 755–771.
[19] D.M. Webber, C.J. Wheatley, The effect of initial potential energy on the dilution of a heavy gas cloud, Journal of Hazardous Materials 16 (1987) 357–380.